Available online at www.sciencedirect.com
ScienceDirect
Journal of the European Ceramic Society 29 (2009) 2249–2257
www.elsevier.com/locate/jeurceramsoc

Microstructural and in vitro characterisation of high-velocity suspension flame sprayed (HVSFS) bioactive glass coatings

G. Bolelli [a], V. Cannillo [a,*], R. Gadow [b], A. Killinger [b], L. Lusvarghi [a], J. Rauch [b]

[a] *Department of Materials and Environmental Engineering, University of Modena and Reggio Emilia, Via Vignolese 905, I-41100 Modena (MO), Italy*
[b] *Institute for Manufacturing Technologies of Ceramic Components and Composites (IFKB), Universität Stuttgart, Allmandring 7b, D-70569 Stuttgart, Germany*

Received 7 December 2008; received in revised form 19 January 2009; accepted 30 January 2009
Available online 6 March 2009

Abstract

The paper reports the first attempt at employing the innovative high-velocity suspension flame spraying (HVSFS) technique in order to deposit bioactive glass coatings. Fine (micrometric) glass particles having a composition similar to that of the A–W (apatite–wollastonite) bioactive glass–ceramic as proposed by Kokubo were dispersed into a 50% water + 50% isopropanol solvent mixture and the resulting suspension (containing 20 wt.% glass powder) was thermally sprayed onto Ti plates using a modified high velocity oxy-fuel torch.

Each torch pass produces a dense coating layer, featuring strong cohesion between lamellae thanks to viscous flow sintering along the interlamellar boundary. However, some porosity exists between different layers deposited during successive torch passes.

In vitro bioactivity tests indicate that the coatings interact remarkably with the simulated body fluid (SBF), developing a thick silica-rich layer containing hydroxyapatite crystals.

Keywords: High-velocity suspension flame spraying (HVSFS); Bioactive glass coatings; In vitro tests; Coating porosity

1. Introduction

SiO_2–CaO–P_2O_5-based bioactive glasses and glass–ceramics are attractive materials for biomedical applications, because of the excellent levels of bioactivity which can be achieved by formulating and selecting appropriate compositions.[1,2]

Bioactive glasses (and glass–ceramics) can indeed elicit complex, multi-stage interactions with living body fluids and living tissues, whereby the surface of the component undergoes chemical and structural alterations which subsequently favour the growth of bone tissues. The glassy network of these materials, which contains a weak network former (P_2O_5) and a certain amount of network modifiers, can be partly dissolved by body fluids, thus releasing Ca^{2+} and P^{5+} ions, as well as Si-(OH) groups. Si-(OH) groups subsequently polymerise on the surface of the bioglass–based component and originate a film, whose thickness is typically some tens of micrometers. On the surface of this film, a thin layer of hydroxyl–carbonyl–apatite nucleates and grows, because the fluid becomes locally supersaturated with Ca^{2+} and P^{5+} ions. This layer promotes the adhesion of stem cells, which develop into new bone tissue bonded to the surface of the glass; indeed, the layer has a chemical and structural affinity to bone tissues.[1,2] Moreover, it has been suggested that the release of Si ions into the solution can stimulate intracellular reactions which further assist the preferential development and bonding of bone tissues to the surface of the bioactive glass.[3] Bioactive glasses can therefore act as osteoproductive materials, i.e. they could stimulate bone tissue formation at the intracellular level, not only at the extracellular level.[1]

Due to these favourable characteristics, bioactive glasses and glass–ceramics are already being applied in the biomedical field for the production of sintered bulk components for bone replacement.[1,2,4] *In vivo* laboratory experiments as well as clinical evidence indicate that sintered bulk bioactive glasses and glass–ceramics achieve stronger bonds to bone than sintered bulk hydroxyapatite, whose interaction mechanisms with the human body are very different than those described above.[1,2,4,5]

However, sintered glass and glass–ceramic components (similarly to sintered hydroxyapatite components) cannot be

* Corresponding author.
E-mail address: valeria@unimore.it (V. Cannillo).

0955-2219/$ – see front matter © 2009 Elsevier Ltd. All rights reserved.
doi:10.1016/j.jeurceramsoc.2009.01.032

employed as bone replacement in load-bearing applications, because of their limited mechanical strength and intrinsic brittleness: they are being mainly adopted in oral surgery, ear surgery and iliac crest restoration.[1,2,6]

Load-bearing orthopaedic prostheses, like hip replacements, are normally made of metallic materials, typically Ti and its alloys, tanks to their mechanical strength, relatively low density and bio-inertness, i.e. they do not cause toxic reactions by the human body. In order to promote osteointegration, these prostheses are coated with hydroxyapatite.[1,2,6–8] These coatings, which are industrially applied by the plasma spraying technique, are now generally preferred over the use of PMMA-based bone cement, as they can provide better long-term stability and do not cause adverse responses by the body.[1,2,9] However, plasma-sprayed hydroxyapatite coatings are also associated with some disadvantages. For instance, during the plasma-spraying process, hydroxyapatite (which displays incongruent melting) decomposes into various calcium phosphate phases, including tricalcium-phosphate (TCP) and tetracalcium-phosphate (TTCP), and even to CaO in some cases, and tends to produce amorphous phases upon splat quenching. In order to prevent excessive decomposition of the original material, spray conditions must be accurately tailored and carefully monitored, and a certain amount of unmelted material must be preserved,[10–12] leading to porous coatings having lower average mechanical strength and lower Weibull modulus. Moreover, as the degree of crystallinity of a hydroxyapatite coating controls its bioactivity and bioresorption, in some cases a degree of crystallinity can be required and can only be obtained by performing a post-process heat treatment.[12–16] Such heat treatment increases the process cost and time and, most importantly, it can affect the structure and mechanical properties of the titanium alloy and/or it can cause some geometrical distortions.

As bioactive glasses and glass–ceramics in bulk form have displayed better bioactivity than hydroxyapatite, they can potentially be a suitable replacement for hydroxyapatite also as a coating on metallic prostheses.[1,2,17–21] Compared to hydroxyapatite, a bioactive glass does not undergo phase alteration or compositional alteration during thermal spraying; indeed, previous experiments have shown that plasma-sprayed glasses (including both bioactive glasses [19] and glasses for other applications [22]) retain their glassy structure and do not change their chemical composition.

Thermal spraying appears again as the most viable technique for the deposition of bioactive glass coatings on metallic prostheses: compared to other technologies (like sol–gel processing, laser processing, dip-coating, electrophoretic deposition), thermal spraying is fast, flexible, and does not necessarily require high-temperature post-process heat treatments.[18] Moreover, compared to techniques like the pulsed laser deposition, it enables the production of relatively thick coatings: it has been shown that, if a bioactive glass coating is too thin, the dissolution and polymerisation reactions described previously can involve the whole coating thickness, thus compromising its adhesion to the substrate.[23]

This paper reports the first attempt of depositing bioactive glass coatings using an innovative thermal spraying technique, namely the high-velocity suspension flame spraying (HVSFS) technique.[24,25] It was seen as a fundamental so far that thermal spraying requires powder materials with congruent melting behaviour to match and to control the spray deposition process. Amorphous and non-crystalline materials were hardly used in supersonic flame and plasma spraying because of the principal problems of heat transfer and phase stability during the solid-liquid-solid transition in thermal spray deposition.

In the novel HVSFS process,[24,25] a gas-fuelled high velocity oxygen-fuel (HVOF) torch has been modified in order to enable the direct axial injection of liquid suspensions instead of dry powders. Thus, the adoption of very fine (micrometric) particles, whose flowability in dry form is too poor for conventional thermal spraying processes, becomes possible. Fine particles are easy to melt and result in very thin splats; accordingly, coatings possess very low porosity and high strength.[26,27] The HVSFS technique has already been proven to be able to deposit very dense glass coatings, having superior mechanical properties to those of atmospheric plasma sprayed (APS) ones,[28] so that it can certainly be a viable technique to deposit improved bioactive glass coatings as well.

The glass composition which was selected for this first test was the one developed by Kokubo et al. [5,29,30] and generally known as A–W. This composition potentially enables a large flexibility in the tailoring of the structural and microstructural characteristics of the coating. Indeed, this composition can form a glass–ceramic containing apatite and wollastonite when treated at a suitable temperature: both the parent glass and the apatite–wollastonite glass–ceramic are bioactive.[5,29,30] Therefore, the as-deposited coating can be expected to have a purely glassy structure, and is expected to be bioactive. By performing an optional post-process heat treatment, the coating could be turned into a glass ceramic and its functional characteristics modified. Thus, a bioactive coating can be obtained with no mandatory need for post-deposition heat treatments. If technical and economical considerations on the specific applications indicate the heat treatment is affordable, it can be optionally performed in order to modify the coating's behaviour.

2. Materials and methods

2.1. Powder production and characterisation

A glass having a composition similar to the A–W glass reported by Kokubo et al. [5,29,30] (Table 1) was produced using industrially available raw materials of SiO_2, $MgCO_3$, $CaCO_3$, $Ca_3(PO_4)_2$ and CaF_2. A frit was obtained by melting the batch in a platinum crucible using an electric furnace at 1550 °C for 1 h, and by casting it into water. The frit was dry milled in a fast planetary moving mill, using Al_2O_3 balls (20 mm and 10 mm diameter), and then sieved below 45 μm. A suspension consisting of 20% sieved glass powder and 80% water + isopropanol mixture (50 wt.% H_2O, 50 wt.% isopropanol) was prepared by attrition-milling with 6 mm diameter ZrO_2 balls for 7 h. The average powder size could therefore be further reduced.

The chemical composition of the sieved glass powder was assessed by inductively coupled plasma-optical emission spec-

Table 1
Nominal and actual composition of the glass frit employed in this work (in weight %).

	SiO_2	P_2O_5	CaO	CaF_2	Al_2O_3	MgO
Nominal composition of Kokubo[5]	34	16.2	44.7	0.5	–	4.6
Actual composition	33.30	13.30	48.20	0.03	1.90	1.92

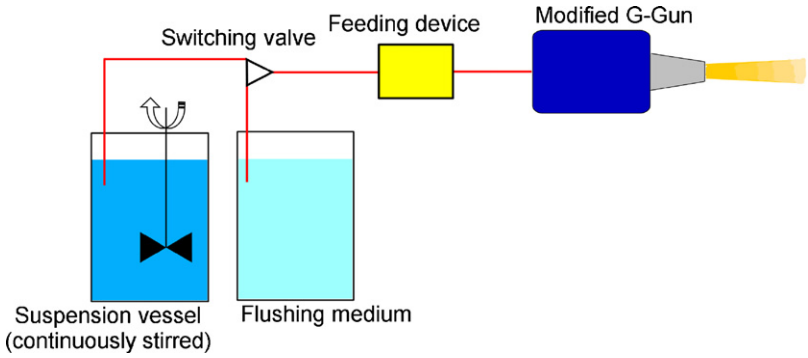

Fig. 1. Layout of the HVSFS system.

trometry (ICP-OES, Liberty-Varian 500, Varian Inc, Palo Alto, CA, USA). The particle size distribution of the powder was measured by the laser diffraction technique both after sieving, prior to attrition milling (Mastersizer 2000, Malvern Instruments Ltd., Worcestershire, UK), and after attrition milling (Getzmann GmbH). The thermal behaviour of the glass powder was characterised by means of differential thermal analysis (DTA, DSC-404, Netzsch GmbH, Selb, Germany) in the 20–1100 °C range (heating rate: 10 °C/min), in order to assess the glass transition and crystallisation temperatures (T_g, T_c). The density of the glass was measured by He picnometry (AccuPyc 1330, Micromeritics s.r.l., Peschiera Borromeo (MI), Italy). Sintering tests on pressed powders were carried out with a hot stage microscope (Misura HSM ODHT, Expert System Solutions, Modena, Italy) to find the sintering temperature of the frit. The thermal expansion coefficient of the glass was measured by mechanical dilatometry (DIL 404, Netzsch) on (15 mm × 5 mm × 5 mm) glass bars, which were machined from bulk glass samples, produced by casting the molten glass into a carbon mould and subsequently annealed at 760 °C for 1 h.

2.2. Coating deposition and characterisation

The attrition-milled suspension was sprayed onto (50 mm × 50 mm × 3 mm) Ti plates by the HVSFS process.[24,25,27–28] As shown in Fig. 1, the suspension, stored in a vessel and mechanically stirred along the whole process duration, is fed to the torch (a G-Gun torch, GTV GmbH, Luckenbach, Germany) using a suitable feeding system, capable of providing a uniform and controlled suspension flow rate. In the HVOF torch, the powder injector is replaced by a conical suspension injector, coaxial with the combustion chamber and ending with a 0.3 mm diameter orifice. A specially designed 22-mm long conical combustion chamber with a 135-mm long expansion nozzle was fitted to the torch. The spray parameters, chosen after some preliminary tests aimed to achieve good deposition efficiency, are listed in Table 2. The Ti plates were cleaned with isopropanol and grit-blasted using 200 μm alumina grits at 5 bar pressure, immediately before spraying.

The polished cross-sections of the coatings (mounted in resin, ground with 800, 1000, 2000 mesh SiC papers and polished with 3 μm and 0.5 μm poly-crystalline diamond suspension) and their fractured sections (obtained by cryogenic fracture in liquid N_2) were observed by scanning electron microscopy (ESEM Quanta-200, FEI, Eindhoven, The Netherlands) coupled with energy dispersion X-ray spectrometry (EDS, INCA 350, Oxford Instruments, Abingdon, UK). X-ray diffraction (X'Pert Pro, PANAlytical, Eindhoven, The Netherlands) was performed on the coatings' surfaces in the [15°, 70°] 2θ range, at a scan speed of 2°/min, (0.02° increment), using Cu Kα radiation at 40 kV and 40 mA.Vickers microhardness (Wilson Wolpert MVD402 microhardness tester) was measured on polished cross-sections (25 g load, 15 indentations for each sample).

2.3. In vitro testing

The in vitro study was performed using samples of (5 mm × 4 mm × 3 mm), which were cut from the coated plates and soaked in simulated body fluid (SBF), according to the procedure described in Ref. [31]. The soaking tests were carried out in plastic containers immersed in a thermostatic bath at 37 °C.

Table 2
HVSFS deposition parameters.

Propane flux (Sl/min)	40
Oxygen flux (Sl/min)	350
Spray distance (mm)	140
Traverse speed (mm/s)	400
Pass distance (mm)	2
Number of cycles	5
Cooling	Compressed air jets

The samples were placed in vertical position inside the containers (according to the procedure described in Ref. [31]). Soaking times were 1, 2 and 5 weeks; for each test duration, two samples were tested. Prior to immersion, the samples were weighed with ±0.1 mg accuracy.

After the extraction, the samples were rinsed in double-distilled water and dried at room temperature. The pH of the test solution was measured by a pH-meter (MicroPH 2001, Crison Instruments SA, Barcelona, Spain) after each soaking interval, at a temperature of about 33 °C; its chemical composition was assessed by ICP-OES.

The surface and polished cross-sections of the soaked samples were observed by environmental scanning electron microscopy (ESEM) coupled with energy dispersive spectrometry (EDS). X-ray diffraction was performed on the coatings' surfaces after soaking in SBF, in the same conditions listed above.

3. Results and discussion

3.1. Characterisation of powders and bulk glasses

The actual chemical composition of the milled and sieved glass frit is listed in Table 1: due to the use of industrial raw materials, the real composition is slightly different from the nominal one and, in particular, a small amount of Al_2O_3 is present. The MgO and P_2O_5 percentages are somewhat lower than the nominal composition. The glass has a density of (2.9172 ± 0.0003) g/cm^3. DTA indicates that the glass transition temperature T_g is around 720 °C (Fig. 2); moreover, two definite exothermal crystallization peaks appear at 891 °C and 942 °C. Following previous literature reports, the first peak can be assumed to correspond to the formation of mixed oxy-apatite and fluoroapatite crystalline phases, whereas the second one corresponds to the formation of β-wollastonite.[30] The sinter-

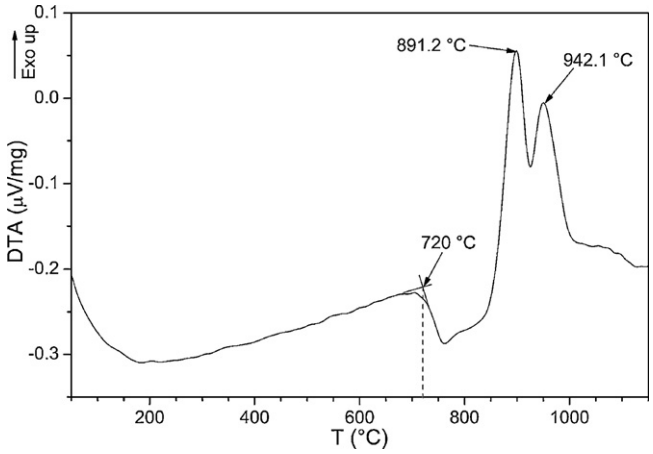

Fig. 2. Differential thermal analysis of the glass powder.

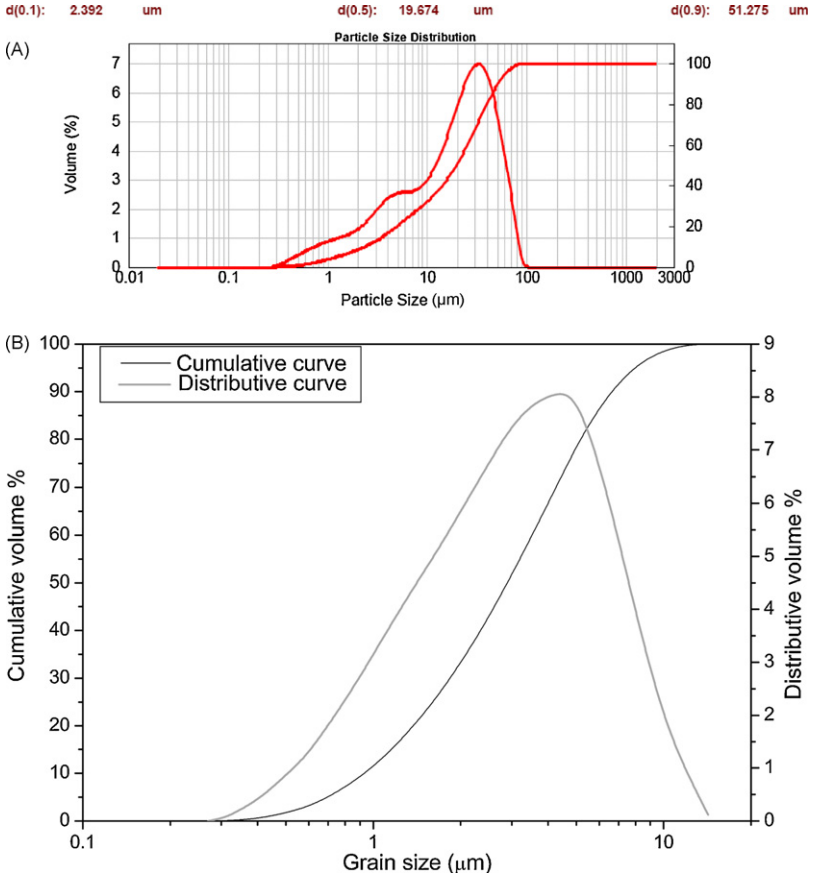

Fig. 3. Particle size distribution of the glass powders: (A) after ball milling and sieving; (B) after attrition milling.

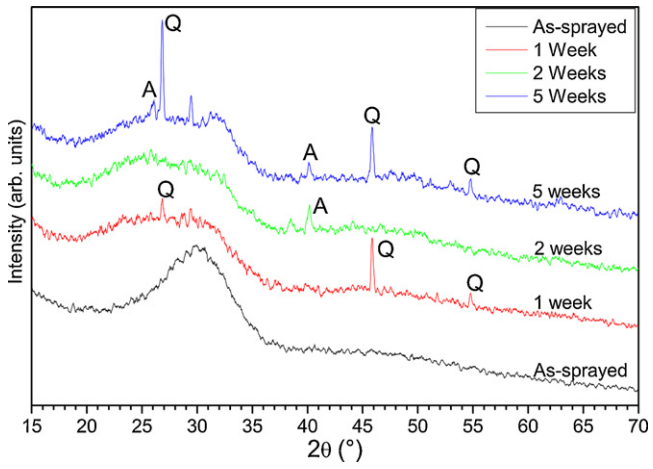

Fig. 4. XRD patterns of AW coating after soaking in SBF: 0, 1, 2 and 5 weeks. Legend: Q = quartz (JCPDS 88-2487), A = hydroxyapatite (JCPDS 73-1731).

ing temperature is about 850 °C and the softening temperature is about 1140 °C, as determined from the hot-stage microscope measurements.

The linear thermal expansion coefficient (50 °C < T < 400 °C) of the glass is 10.08×10^{-6} °C^{-1}, not too far from the thermal expansion coefficient of Ti, which is reported to be 9.70×10^{-6} °C^{-1} in the 50 °C < T < 540 °C range.[32]

After ball milling and sieving, the glass powder has an average particle size of about 20 μm (Fig. 3A); the subsequent attrition milling stage is very effective in reducing the average particle size down to about 3 μm (Fig. 3B). This particle size is perfectly suited to the HVSFS technique and can be expected to result in small, thin lamellae, suitable to reduce porosity and pore size of the sprayed coating.

3.2. Microstructure of the coatings

XRD patterns confirm that the as-deposited coating is completely glassy (Fig. 4). On the polished cross-sections of this coating (which is about 100 μm thick), lamellae boundaries are hardly perceivable (Fig. 5). Individual, flattened lamellae are difficult to discern even on fracture surface views (Fig. 6A): only at few locations can they be identified (Fig. 6B, see circle). This means that brittle fractures do not propagate preferentially along these boundaries. Where such lamellae are recognizable, their diameter seems to be always ≤5 μm: as the typical splat flattening ratio in suspension thermal spraying is about 2,[33] the lamellae were originated by fully molten glass droplets whose size never exceeds 3 μm. This value is comparable to the average equivalent diameter of individual attrition-milled glass particles (Fig. 3B), thus suggesting that most of those particles melted separately inside the gas jet. It is likely that only the finest ones (those smaller than 1 μm) were agglomerated and melted together. Consistently, previous numerical simulations indicated that the strong turbulence inside an HVOF gas jet would disrupt a liquid drop into droplets of a few microns diameter.[34] Such droplets can only contain one or very few attrition-milled glass particles.

In accordance to the lack of clearly recognizable lamellae, no longitudinally elongated interlamellar pores can be detected in SEM micrographs (Fig. 5A, B), too. The most recurring porosity features are small, rounded pores (Fig. 5A, B), which are generally believed to be caused by gas entrapment within molten material.[35] However, a careful inspection of SEM micrographs indicates that these rounded pores tend to concentrate mainly along the boundaries between two successive torch passes; indeed, the five layers produced by the 5 torch cycles (Table 2) can be recognized by following the arrangement of the globular pores, as indicated by dashed lines in Fig. 5A. Inside each layer, by contrast, there are fewer rounded pores (Fig. 5A, B), but some transverse microcracks exist (Fig. 5B). Fractured section views confirm that, above and below each of these layers of strongly coherent lamellae, rounded pores appear (Fig. 6A–C). It worth noting that these pores are mainly due to the presence of non-flattened, hollow spherical particles: part of the pores is due to the spherical cavities inside these particles, whereas part is due to imperfect overlapping between these non-flattened particles (Fig. 6B, C: see arrows). Non-flattened particles are also clearly perceivable on the surface of the HVSFS glass coatings (Fig. 6D): an analogous surface morphology has already been reported for other HVSFS-deposited glass coatings.[28]

These rounded particles have a diameter ranging from ≤1 μm to a few microns; therefore, the previous observations on the lack of a significant agglomeration between the individual attrition-milled glass particles during thermal-spraying are confirmed. Similarly to the flattened lamellae, the rounded particles were originated by individual micron-sized particles; only those smaller than 1 μm could possibly have agglomerated during spraying.

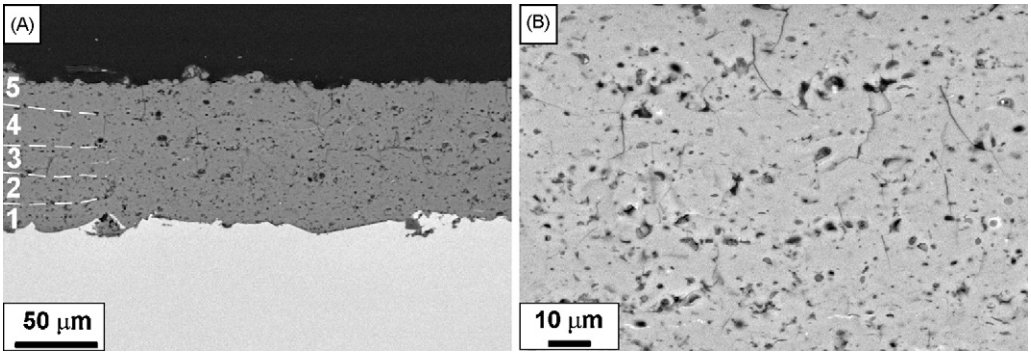

Fig. 5. SEM cross-sections of as-sprayed AW coating: (A) general view (400×), highlighting the 5 torch passes; (B) detail (1000×).

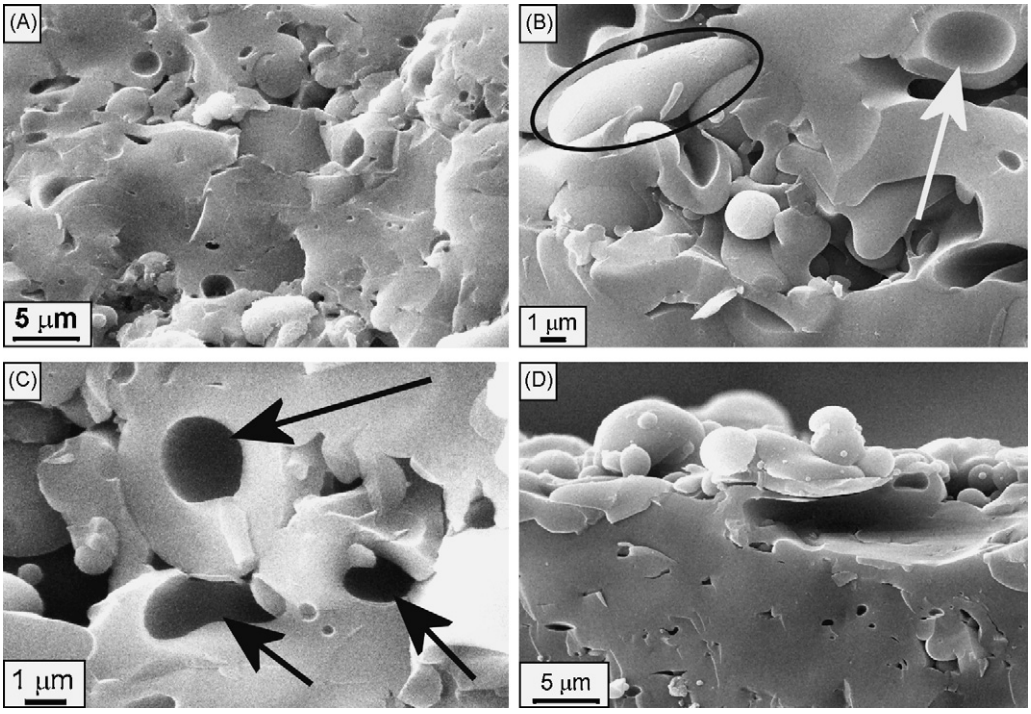

Fig. 6. Fractured sections of HVSFS-deposited AW coatings. (A) General view; (B, C) details (circle: flattened lamella; arrows: rounded particles with central pore); (D) view near the coating's surface.

The mechanism which probably governs the build-up of glass coatings during HVSFS deposition has been proposed in Ref. [28]. The HVSFS gas jet rapidly heats the very small glass particles well above the glass transition temperature. Due to the low inertia and low thermal capacity of small, micrometric particles, their in-flight velocity and temperature histories tend to reproduce the velocity and temperature profiles of the gas jet,[36] differently from larger particles which are capable of retaining their velocity and temperature along a certain flight distance.[36,37] Accordingly, the spray distance, which is typically about or above 200 mm in conventional gas-fuelled HVOF spraying, was reduced to 140 mm in this case; therefore, many particles still possess high velocity and high temperature (above T_g) when they reach the substrate. The glass particles impacting on the substrate at $T > T_g$ can spread by viscous flow, so they flatten extensively. Moreover, when two or more particles having $T > T_g$ reach the substrate almost at the same time, viscous flow sintering can occur along their boundary, thus explaining the excellent inter-lamellar cohesive strength inside each HVSFS-deposited layer. When a layer consisting of strongly bonded sintered lamellae cools down below T_g, because of the compressed air jet cooling as well as because of natural convection, tensile stresses are developed, causing the formation of transverse microcracks inside the layer (Fig. 5B).

The smaller particles and/or the particles which may tend to escape from the centreline of the gas jet, however, might become slow and cold before reaching the substrate. A particle whose temperature is around or below T_g might be prevented from flattening properly upon impact, as its viscosity is already quite large. If the particle had entrained some gas as it attained the highest in-flight temperatures, a gas bubble can be entrapped in the particle itself. The improper flattening of cold particles and the entrainment of gas bubbles inside them can explain the porosity features noted both on polished and on fractured sections. As these particles are not only colder, but also slower than the other particles, they will reach the substrate a few instants after the faster and well-melted particles, thus forming a thin defective film on top of each layer deposited by a single torch cycle. This mechanism would explain why most of the rounded pores concentrate along the boundaries between adjacent layers. At the end of the last cycle, these rounded particles remain clearly visible on the top surface of the coating.

The Vickers microhardness of the coating is (2.42 ± 0.29) GPa.

3.3. In vitro test and characterisation

A SiO_2-rich layer of about 10 μm is observed by SEM on the surface of the AW coating after soaking in SBF for 1 week (Fig. 7A, EDS microanalysis in Fig. 8). This layer is partly crystalline, as XRD patterns reveal the presence of quartz peaks (JCPDS 88-2487: Fig. 4, label Q) after the first week of immersion in SBF. The thickness of the SiO_2-rich layer increases significantly with the soaking time, reaching about 30 μm and 70 μm of thickness after 2 and 5 weeks, respectively (Fig. 7B, C). After 1 week, a uniform apatite layer on top of the silica-rich layer is not observed. By contrast, after 2 weeks of soaking, some bright areas can be observed inside the SiO_2-rich layer (Fig. 7B), and many more appear after 5 weeks of soaking (Fig. 7C). They are apatite-rich regions; indeed, EDS spectra reveal that these bright areas are rich in Ca and P (Fig. 8): the Ca/P ratio is about 1.76 and 1.45 after 2 and 5 weeks of soaking, respectively.

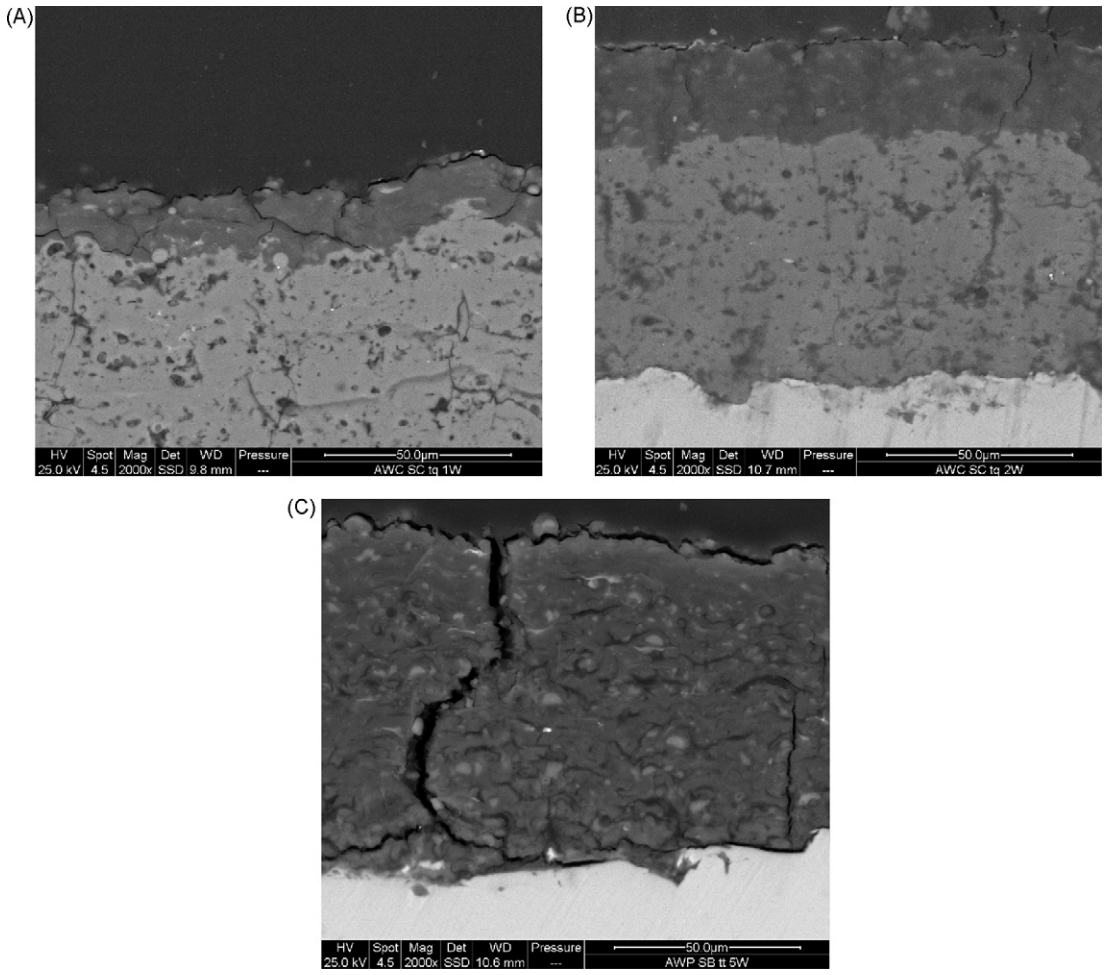

Fig. 7. SEM cross-sections of AW coating after soaking in SBF for 1 week (A), 2 weeks (B) and 5 weeks (C).

The Ca/P ratio of a crystalline hydroxyapatite should be about 1.67, from ISO 13779-3. If the semi-quantitative nature of the EDS technique is taken into account, it can therefore be inferred that these bright area are, most likely, apatite-based areas. Consistently, X-ray diffraction peaks related to the hydroxyapatite phase (JCPDS 073-1731: Fig. 4, label A) start being noticeable after the second week. After the fifth week of soaking the intensity of the hydroxyapatite and of the quartz peaks increases.

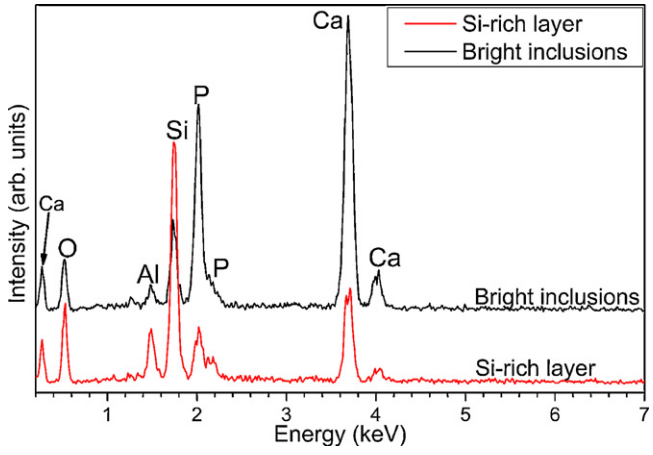

Fig. 8. EDS spectra of the SiO_2-rich layer and of the bright areas seen after 2 and 5 weeks of SBF soaking.

Transverse and longitudinal cracks are also formed in the coating. They may be a consequence of the chemical alteration of the coating during the interaction with the SBF solution, but some could also be an artefact due to the metallographic cutting and polishing procedures.

These deep microstructural and structural alterations of the coating are coupled to some change in the pH of the solution (Fig. 9). The glassy network is indeed chemically attacked by the SBF, as anticipated in the Introduction: ions (especially Ca^{2+} ions) are rapidly leached out of the network, as confirmed by the chemical analysis of the test solution after 1 week (Fig. 10). Consequently, the whole glassy network is altered and Si is also released to the SBF solution (Fig. 10).

These observations are consistent with the interactions mechanisms between SBF and bioactive glasses, proposed in the pertinent literature:[1–4] Si–(OH) groups are released from the glass as a consequence of the network dissolution and subsequently precipitate and polymerise on the surface of the glass itself, thus forming the silica-rich film observed in SEM micrographs.

The leaching of Ca^{2+} ions also leads to supersaturation of the fluid in the vicinity of the bioactive glass coating: this is the most

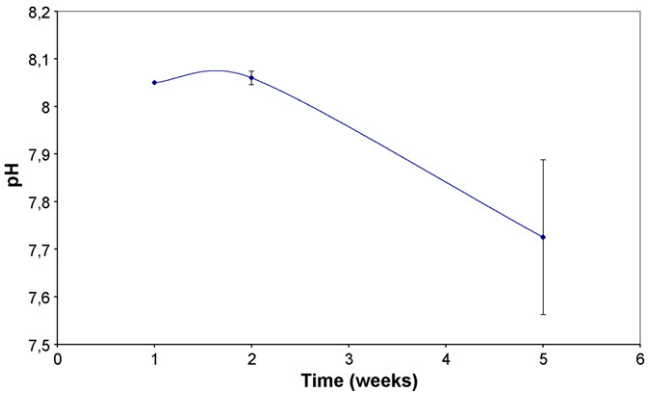

Fig. 9. Evolution of the pH of the SBF solution as a function of the soaking time of the AW coating.

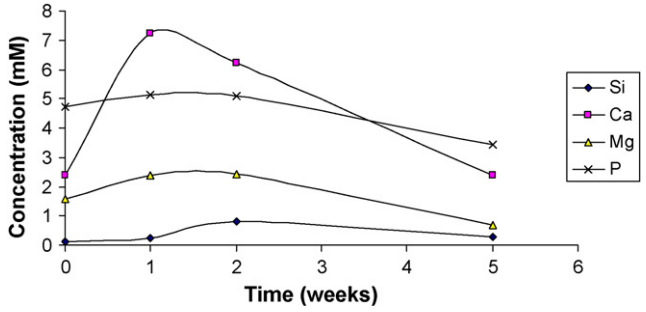

Fig. 10. Concentrations of Si, Ca, Mg and P (mM) in the SB solution as a function of the soaking time of the AW coating.

probable cause of the precipitation of hydroxyapatite [29] during the second week of soaking, as noted from SEM micrographs and XRD patterns. Accordingly, after the initial increase, the Ca concentration decreases from the first to the second week, and continues to decrease until the fifth week (Fig. 10).

The increase in P concentration during the first week is much lower than that of Ca, and, at the end of the test, the concentration of P in the solution is lower than the initial concentration in the SBF (Fig. 10). It has indeed been suggested that P for the formation of hydroxyapatite mostly comes from the solution itself, rather than from the dissolution of the glassy network [29].

4. Conclusions

The HVSFS technique was employed in order to deposit A–W bioactive glass coatings onto titanium plates. The technique seems capable of providing good quality coatings, having limited porosity and showing excellent interlamellar cohesion within each layer. However, further improvements in the coatings' quality could be obtained by optimizing the deposition parameters in order to minimize the amount of cold, slow particles, which generate interlayer defects.

The deposited layers display a remarkable activity in simulated body fluid, with the formation of a silica-rich layer and of hydroxyapatite crystals. However, unlike common bioactive glasses,[1–3] hydroxyapatite does not appear as a thin film on top of the silica-rich layer, but rather as regions dispersed inside each layer.

Moreover, as the HVSFS technique appears to be suitable for the deposition of good-quality bioactive glass coatings, other compositions having different interaction mechanisms with simulated body fluids can certainly be selected.

Acknowledgments

The authors are grateful to Ms. Fiorenza Pierli and to Mr. Sandro Pizzolante for their precious assistance with the in vitro tests and to Dr. Maria Cannio for the ICP-OES chemical analyses. This work was partially supported by MIUR (Funds "Programmi per l'incentivazione del processo di internazionalizzazione del sistema universitario").

References

1. Cao, W. and Hench, L. L., *Bioactive Materials, Ceramics International*, 1996, **22**, 493–507.
2. Hench, L. L., *Bioceramics, Journal of the American Ceramic Society*, 1998, **81**, 1705–1728.
3. Carlisle, E., *Silicon Biochemistry*. J. Wiley, Sons Inc., NY, USA, 1986, p. 123–136.
4. Höland, W., Biocompatible and bioactive glass–ceramics - state of the art and new directions. *Journal of Non-Crystalline Solids*, 1997, **219**, 192–197.
5. Nakamura, T., Yamamuro, T., Higashi, S., Kokubo, T. and Itoo, S., A new glass–ceramic for bone replacement: evaluation of its bonding to bone tissue. *Journal of Biomedical Materials Research*, 1985, **19**, 685–698.
6. Gross, K. A. and Berndt, C. C., *Biomedical Application of Apatites Phosphates: Geochemical Geobiological Materials Importance—Reviews in Mineralogy Geochemistry*, *48*, ed. M. J. Kohn, J. Rakovan and J. M. Hughes. Mineralogical Society of America, Washington, DC, USA, 2002, pp. 631–672.
7. Liu, X., Chu, P. K. and Ding, C., Surface modification of titanium, titanium alloys, and related materials for biomedical applications. *Materials Science and Engineering R*, 2004, **47**, 49–121.
8. Sun, L., Berndt, C. C., Gross, K. A. and Kucuk, A., Material fundamentals and clinical performance of plasma-sprayed hydroxyapatite coatings: a review. *Journal of Biomedical Materials Research*, 2001, **58**, 570–592.
9. Mallory, T. H., William, C., Head, M. D., Lombardi, V. A., Emerson, R. H., Eberle, R. W. *et al.*, Clinical and radiographic outcome of a cementless, titanium, plasma spray-coated total hip arthroplasty femoral component: justification for continuance of use. *The Journal of Arthroplasty*, 1996, **11**, 653–660.
10. Sun, L., Berndt, C. C., Khor, K. A., Cheang, N. H. and Gross, K. A., Surface characteristics and dissolution behavior of plasma-sprayed hydroxyapatite coating. *Journal of Biomedical Materials Research*, 2002, **62**, 228–236.
11. Dyshlovenko, S., Pawlowski, L., Roussel, P., Murano, D. and Le Maguer, A., Relationship between plasma spray operational parameters and microstructure of hydroxyapatite coatings and powder particles sprayed into water. *Surface & Coatings Technology*, 2006, **200**, 3845–3855.
12. Dyshlovenko, S., Pawlowskia, L., Pateyron, B., Smurov, I. and Harding, J. H., Modelling of plasma particle interactions and coating growth for plasma spraying of hydroxyapatite. *Surface & Coatings Technology*, 2006, **200**, 3757–3769.
13. Pierlot, C., Pawlowski, L., Tomaszek, R., Dyshlovenko, S. and Bigan, M., Interdependence of different properties of hydroxyapatite coatings and powders plasma sprayed into water. *Chemometrics and Intelligent Laboratory Systems*, 2007, **86**, 153–158.
14. Dyshlovenko, S., Pierlot, C., Pawlowski, L., Tomaszek, R. and Chagnon, P., Experimental design of plasma spraying and laser treatment of hydroxyapatite coatings. *Surface & Coatings Technology*, 2006, **201**, 2054–2060.
15. Yang, C.-W., Lee, T.-M., Lui, T.-S. and Chang, E., Effect of post vacuum heating on the microstructural feature and bonding strength of plasma-sprayed hydroxyapatite coatings. *Materials Science and Engineering C*, 2006, **26**, 1395–1400.

16. Lugscheider, E., Knepper, M. and Nyland, A., Characterization of thermal sprayed bioactive coatings. *Colloids and Surfaces B: Biointerfaces*, 1996, **6**, 1–7.
17. Lopez-Estebana, S., Saiz, E., Fujino, S., Oku, T., Suganuma, K. and Tomsia, A. P., Bioactive glass coatings for orthopedic metallic implants. *Journal of the European Ceramic Society*, 2003, **23**, 2921–2930.
18. Zhao, Y., Chen, C. and Wang, D., The current techniques for preparing bioglass coatings. *Surface Review and Letters*, 2005, **12**, 505–513.
19. Gabbi, C., Cacchioli, A., Locardi, B. and Guadagnino, E., Bioactive glass coating: physicochemical aspects and biological findings. *Biomaterials*, 1995, **16**, 515–520.
20. Verné, E., Ferraris, M., Ventrella, A., Paracchini, L., Krajewski, A. and Ravaglioli, A., Sintering and plasma spray depositino of bioactive glass–matrix composites for medical applications. *Journal of the European Ceramic Society*, 1998, **18**, 363–372.
21. Schrooten, J. and Helsen, J. A., Adhesion of bioactive glass coatings to Ti_6Al_4V oral implant. *Biomaterials*, 2000, **21**, 1461–1469.
22. Bolelli, G., Lusvarghi, L., Manfredini, T. and Siligardi, C., Influence of the manufacturing process on the crystallization behavior of a CZS glass system. *Journal of Non-Crystalline Solids*, 2005, **351**, 2537–2546.
23. Borrajo, J. P., Gonzáles, P., Liste, S., Serra, J., Chiussi, S., León, B. *et al.*, The role of the thickness and the substate on the in vitro bioactivity of silica-based glass coatings. *Materials Science and Engineering C*, 2005, **25**, 187–193.
24. Killinger, A., Kuhn, M. and Gadow, R., High-velocity suspension flame spraying (HVSFS), a new approach for spraying nanoparticles with hypersonic speed. *Surface and Coatings Technology*, 2006, **201**, 1922–1929.
25. Gadow R., Killinger A., Kuhn M. and López D., Hochgeschwindigkeitssuspensionsflammspritzen, German Patent DE 10 2005 038 453 A1, Anmeldetag: 03.08.2005, Offenlegungstag: 08.02.2007.
26. Gadow, R., Kern, F. and Killinger, A., Manufacturing technologies for nanocomposite ceramic structural materials and coatings. *Materials Science and Engineering B*, 2008, **148**, 58–64.
27. Gadow, R., Killinger, A. and Rauch, J., New results in high velocity suspension flame spraying (HVSFS). *Surface and Coatings Technology*, 2008, **202**, 4329–4336.
28. Bolelli, G., Rauch, J., Cannillo, V., Killinger, A., Lusvarghi, L. and Gadow, R., Investigation of high-velocity suspension flame sprayed (HVSFS) glass coatings. *Materials Letters*, 2008, **62**, 2772–2775.
29. Kokubo, T., Bioactive glass ceramics: properties and applications. *Biomaterials*, 1991, **12**, 155–163.
30. Kokubo, T., Ito, S., Sakka, S. and Yamamuro, T., Formation of a high-strength bioactive glass–ceramic in the system $MgO–CaO–SiO_2–P_2O_5$. *Journal of Materials Science*, 1986, **21**, 536–540.
31. Kokubo, T. and Takadama, H., How useful is SBF in predicting in vivo bone bioactivity? *Biomaterials*, 2006, **27**, 2907–2915.
32. www.matweb.com (19/03/2008).
33. Fauchais, P., Rat, V., Coudert, J.-F., Etchart-Salas, R. and Montavon, G., Operating parameters for suspension and solution plasma-spray coatings. *Surface and Coatings Technology*, 2008, **202**, 4309–4317.
34. Basu, S. and Cetegen, B. M., Modeling of liquid ceramic precursor droplets in a high velocity oxy-fuel flame jet. *Acta Materialia*, 2008, **56**, 2750–2759.
35. Sobolev, V. V., Guilemany, J. M. and Nutting, J., *High Velocity Oxy-fuel Spraying; Theory, Structure–Property Relationships and Applications*. Maney for the Instutite of Materials, Minerals and Mining, London, UK, 2004, p. 153–157.
36. Dongmo, E., Wenzelburger, M. and Gadow, R., Analysis and optimization of the HVOF process by combined experimental and numerical approaches. *Surface and Coatings Technology*, 2008, **202**, 4470–4478.
37. Gu, S., McCartney, D. G., Eastwick, C. N. and Simmons, K., Numerical modeling of in-flight characteristics of Inconel 625 particles during high-velocity oxy-fuel thermal spraying. *Journal of Thermal Spray Technology*, 2004, **13**, 200–213.